Normal incidence acoustic insertion loss of perforated plates with bias flow

Vincent Phong[a] and Dimitri Papamoschou
Department of Mechanical and Aerospace Engineering, University of California, Irvine, California 92697, USA

(Received 20 May 2015; revised 8 October 2015; accepted 17 November 2015; published online 24 December 2015)

The transmission of sound at normal incidence through perforated plates with bias flow is investigated experimentally and theoretically over a large parameter space. A specially designed experimental apparatus enabled the measurement of insertion loss with bias flow Mach number up to 0.25. A theoretical model for insertion loss was constructed based on inviscid, one-dimensional wave propagation with mean flow through a single contraction/expansion chamber. The mass end correction of the contraction is modified for hole interaction effects and mean flow. Hydrodynamic losses are modeled using a *vena contracta* coefficient dependent on both perforation geometry and Reynolds number. Losses in acoustic energy that occur in the mixing region downstream of the perforations are modeled as fluctuations in entropy. The proposed model was validated experimentally over a range of plate thickness, porosity, and hole size. The experimental results indicate an increase in insertion loss with increasing frequency, followed by saturation and decline as resonant conditions are established in the perforations. The insertion loss at low frequency increases with increasing Mach number through the perforation. The proposed model captures these trends and its predictions are shown to be more accurate than those of past models.
 [http://dx.doi.org/10.1121/1.4937602]

[JWP] Pages: 3907–3921

I. INTRODUCTION

Perforated plates are employed in various noise control applications, such as automotive exhaust mufflers, turbofan engine liners, and pneumatic bleed valve silencers. Air flow is typically present in these applications, which can augment or reduce the damping effectiveness. The flow speed and incidence with respect to the plane of the perforated plate will vary depending on the application. Liners in turbofan engines contain mean flow predominantly at grazing incidence, where the flow direction is parallel to the surface containing the perforations. Flow that is directed through the perforations is referred to as bias flow. In the linear regime of acoustic excitations, a perforated plate behaves as a low-pass acoustic filter when no mean flow is present. The transmission characteristics are determined by the perforated plate's physical parameters,[1] namely, the porosity, β, plate thickness, l, and hole diameter, d. The addition of bias flow through the perforations introduces potential benefits in the absorptive properties of the plate.

Without bias flow, dissipative effects are negligible for the transmission of small amplitude, high-frequency acoustic waves at normal incidence to the plate.[1] Additional losses in acoustic energy may occur when bias flow is present. The mean flow separates from the perforation rims, forming a shear layer. A fraction of the acoustic wave energy is transferred to the kinetic energy of vortical motions in the shear layer and is ultimately dissipated as heat. This implies a non-isentropic process downstream of the perforated plate, where the transmitted acoustic intensity is modulated by fluctuations in entropy. Mungur and Gladwell[2] linearized the energy equation in terms of entropy and obtained an expression relating entropy fluctuations to acoustic pressure fluctuations. Ronneberger,[3] Alfredson and Davies,[4] Davies,[5] and Cummings[6] applied this concept to a duct containing a sudden expansion. Ronneberger[3] and Cummings[6] provided both experimental measurements and theoretical models of the reflection coefficient for Mach number <0.6 upstream of the expansion. Their results[3,6] indicated a monotonic increase in acoustic energy loss with increasing duct Mach number. Hofmans *et al.*[7] and Durrieu *et al.*[8] developed a quasi-steady model for acoustic response of a circular diaphragm and a perforated plate, respectively, subject to bias flow. Using entropy fluctuations to model the acoustic energy dissipation, their results[7,8] indicated increasing transmission loss with increasing bias flow speed for low frequency excitations.

The acoustic response of perforations with bias flow has alternatively been investigated through the interaction between incident acoustic waves and the vortex layer downstream of the perforations. Howe[9] determined the Rayleigh conductivity of a perforated screen, assuming negligible thickness, low bias flow Mach number, and no interaction between perforations. Jing and Sun[10] modified Howe's work[9] to include plate thickness through an impedance correction. Jing and Sun further supplemented their work numerically[11] using the boundary element method (BEM) to develop a model for the Rayleigh conductivity of a perforated plate. The assumptions involved in their analysis are identical to Howe's work,[9] however they included details of the jet profile geometry. Lee *et al.*[12] used BEM to investigate

[a]Electronic mail: vphong@uci.edu

the acoustic interaction between perforations and found that increasing the porosity decreased the reactance of the plate. Mazdeh and Kashani[13] used commercial software ANSYS CFX to determine the Rayleigh conductivity of a single orifice with bias flow. Mendez and Eldredge,[14] used Large-Eddy Simulation (LES) to model the unsteady behavior of flow near the perforations. They emphasized the need to model the jet profile in order to obtain more accurate predictions of the damping characteristics of perforated plates.

Although numerous investigations have been dedicated to the study of the transmission characteristics of perforated plates with bias flow, only few[12] have addressed the effect of flow on the acoustic interaction between the perforations. Interaction effects were ignored on the basis of low porosity applications.[9–11,13,14] A recent study on the design of a pneumatic bleed valve muffler[15] indicated a parameter space (porosity, Mach number, and acoustic frequency) where previous theoretical models lack validation.[7–14] Perforated plates are used in mufflers for bleed valves on gas turbines.[15] The bleed valves regulate pressure in the compressor of a turbofan engine by discharging air into the fan duct, preventing compressor surge during transients or throttle back. Without a muffler, the valve exhaust forms a high-speed turbulent jet which contributes significantly to the total aircraft noise. Figure 1 depicts schematically the bleed valve assembly. The muffler comprises typically two or more perforated plates that are oriented substantially normally to the mean flow direction. The muffler expands the cross-sectional area of the flow, reducing its bulk velocity. The smaller jets emerging from the perforations generate high-frequency noise that is quickly attenuated by atmospheric absorption. The remaining internal sources of sound, including turbulence and vortex shedding, are transmitted through the perforations. The transmission characteristics of these sources depend on both the perforated plate geometry and mean flow. Phong and Papamoschou[1] constructed a model which detailed the dependence of sound attenuation on the properties of the perforated plate (porosity, hole size, and thickness); however, mean flow was not considered in their work. This formed the motivation for the current study: to extend the work of Phong and Papamoschou[1] to better understand and model the transmission of sound through perforated systems exemplified in Fig. 1.

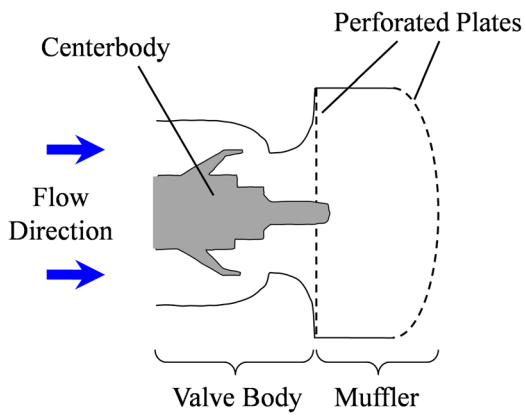

FIG. 1. (Color online) Schematic of pneumatic bleed valve assembly used on aircraft engines (see Ref. 15).

A model for the normal incidence, acoustic insertion loss of a perforated plate subject to low Mach number bias flow is proposed in the present work. The model is based on the one-dimensional analysis conducted by Durrieu *et al.*,[8] using entropy fluctuations to model acoustic energy dissipation due to bias flow. Although the analysis of Durrieu *et al.*[8] does not include detail of acoustic/vortex layer interaction, it offers the simplicity of an analytical solution without the use of numerical methods, which have been the thrust of recent efforts.[11–14] Modifications to the analysis[8] are made to include both acoustic and mean flow interaction between perforations, and the effect of plate thickness. The proposed model is validated experimentally using a broadband noise source, allowing the transmission characteristics to be obtained over a broad spectrum of frequencies in a single experiment run. Insertion loss measurements are obtained for perforated plates over a comprehensive range of porosity, hole diameter, plate thickness, and bias flow speeds. The proposed model will be validated by comparison with experimental results and previous models.

II. THEORETICAL MODELING

A. Fundamental principles

The current investigation focuses on the acoustic insertion loss of perforated plates, namely, the difference in acoustic power measured downstream of the perforated plate, with and without the plate installed. This is a process that is generally governed by inertial and viscous effects. The discriminant between viscous and inertial effects on sound propagation through a short tube is expressed as the ratio of the perforation radius to the acoustic boundary layer thickness

$$\eta = \frac{1}{2} d \sqrt{\frac{\rho\omega}{\mu}}, \tag{1}$$

where d, ω, ρ, and μ are the tube diameter, angular frequency, density and dynamic viscosity of the fluid, respectively. The acoustic boundary layer thickness, $(\mu/\rho\omega)^{1/2}$, in Eq. (1) corresponds to the length scale of laminar harmonic oscillations of a fluid over a flat plate. Crandall[16] determined that the propagation is dominated by viscous effects for $\eta \leq 1$, and that inertial effects become prominent for $\eta > 1$. For a tube diameter of 1 mm (the order of magnitude in this study), and for air at standard conditions, the discriminant becomes $\eta = 0.3165\ (f)^{1/2}$, where $f = \omega/(2\pi)$ is the acoustic frequency. This means that inertial effects dominate down to frequencies on the order of 10 Hz. Aerospace applications are typically concerned with much higher frequencies associated with peak levels of annoyance. Therefore, the sound transmission process can be treated as purely inertial with a good degree of accuracy for the application that motivated this study.

Although viscous damping has negligible influence on the acoustic wave propagation for the applications concerning this study, the effect of viscosity on the mean flow development through the perforations must be included. For perforations with sharp corners, the mean flow separates

from the upstream rim, forming a free jet downstream from each perforation. The mean flow into each perforation has radial velocity component towards the axis of the perforation, causing the jet to contract. The jet cross-sectional area becomes minimum where the streamlines are parallel to the jet axis at the *vena contracta*. The mean flow separation implies a viscous process that is included in the current study through the discharge coefficient (to be detailed in Sec. II C).

The transmission loss (L_T) and insertion loss (L_I) are frequently-used performance criteria of a silencing device. The transmission loss is defined as[17]

$$L_T = 10\log_{10}\left[\frac{\Pi_i}{\Pi_t}\right], \tag{2}$$

where Π is the acoustic power, and the subscripts i and t denote the incident and transmitted waves, respectively. In-duct acoustic measurements of transmission loss are challenging. The incident acoustic wave power is measured upstream of the plate, requiring isolation of the microphone installation to avoid diffraction of the incident acoustic field. The insertion loss is a more convenient performance criterion for experimental measurements, and is defined as

$$L_I = 10\log_{10}\left[\frac{\Pi_{t,0}}{\Pi_t}\right]. \tag{3}$$

Unlike the transmission loss measurement, the insertion loss is a comparison of the sound power at the same location downstream of the perforated plate, with (Π_t) and without ($\Pi_{t,0}$) the plate installed. With appropriate duct insulation, in-duct measurements of insertion loss can be made accurately without installing a microphone upstream of the plate. The insertion and transmission losses are equal if anechoic termination is ensured both upstream and downstream of the plate.[17]

Acoustic disturbances radiating from within the perforations are subject to inertial loading by the surrounding medium. The coupling between disturbances within the perforation and the mass of the surrounding fluid can be modeled as an end correction to the perforation thickness. For plates with low porosity, the perforations are sufficiently separated such that the end correction is approximately equal to the end correction for a single orifice in an infinite baffle.[18] Acoustic interaction between perforations must be modeled for high porosity plates. Fok[19] described the hole interaction effect (HIE) as a correction to the Rayleigh conductivity of a single orifice. An analytical expression known as Fok's function was developed using potential theory (to be introduced in Sec. II C) and can be expressed in terms of the plate porosity β. Nesterov[20] validated Fok's work experimentally, showing that an increase in the porosity corresponds to a reduction in the end correction for thickness. Other investigators attributed HIE to the diffraction of pressure waves that radiate from the perforations. Christensen *et al.*[21] and Hou *et al.*[22,23] concluded that the diffracted waves created acoustic modes that travel parallel to the surface of the perforated plate. The interaction between the surface modes and diffracted pressure waves from the perforations modifies the resonance condition associated with the original plate thickness to a plate that is 16% thinner.[22,23] The aforementioned works[21–23] indicated that HIE results in scaling the end correction associated with a single orifice. In the current investigation, the HIE was accounted for using Fok's function with more details on this implementation presented in Sec. II C.

Concerning the fluid mechanics in the vicinity of the orifice, boundary layer separation from the orifice rim can occur either with bias flow through the perforations or when the pressure fluctuation levels are large enough to produce significant acoustic velocity through the perforation. Cummings and Eversman[24] showed that the mean flow and acoustic velocity contribute linearly and non-linearly, respectively, to the dissipation of a plane acoustic wave traveling with the direction of a free jet. Their analysis[24] indicated that the non-linear contribution from the acoustic velocity can be neglected if $M_2 \gg 0.5|u'|/c_1$, where M_2 and u' are the Mach number acoustic velocity inside the orifice and c_1 is the acoustic wave propagation speed upstream of the orifice. The acoustic velocity magnitude is approximated using the plane wave relation

$$|u'| = \frac{p_{\text{ref}}10^{\text{SPL}/20}}{\rho_1 c_1}, \tag{4}$$

where $p_{\text{ref}} = 20\,\mu$Pa is the reference pressure and sound pressure level (SPL) is the sound pressure level. Sound pressure levels in the experiments of this study were about 60 dB. For air at standard conditions, the quantity $0.5|u'|/c_1 \sim 10^{-7}$. Bias flow Mach numbers are typically at least 0.1 in the applications of this study, and therefore the contribution to dissipation due to non-linear effects are negligible in comparison to the linear contribution of bias flow.

B. Previous models

Howe[9] proposed an analytical model for the Rayleigh conductivity of a circular aperture in an infinitely thin plate subject to low Mach number bias flow. A vortex sheet shed downstream of the aperture was assumed circular and cylindrical in shape. The vortex sheet strength was determined by the condition that u' and p' remain finite at the rim of the aperture. This approach was extended to a perforated screen where the perforations were assumed sufficiently separated to neglect interaction effects. Howe characterized the performance of the perforated plate using the Rayleigh conductivity, which is an equivalent expression for the acoustic admittance

$$K_R = 2a\left\{1 + \frac{\frac{\pi}{2}I_1(St)e^{-St} - iK_1(St)\sinh(St)}{St\left[\frac{\pi}{2}I_1(St)e^{-St} + iK_1(St)\cosh(St)\right]}\right\}. \tag{5}$$

Here $St = \omega a/u_2$ is the Strouhal number based on the bias flow velocity through the aperture, u_2, and the aperture radius, a. I_1 and K_1 are the modified Bessel functions of the first and second kind, respectively. Using the real and imaginary components of Eq. (5) in normalized form, $\gamma_R = \text{Re}\{K_R/(2a)\}$ and $\delta_R = \text{Im}\{K_R/(2a)\}$, respectively, Howe defined the transmission coefficient as

$$T_c = \frac{(4\beta/\pi M_2)(\gamma_R - i\delta_R)}{|St_a + (i4\beta/\pi M_2)(\gamma_R - i\delta_R)|^2}, \quad (6)$$

where the $M_2 = u_2/c$ is the Mach number of the mean flow in the perforations, and c is the wave propagation speed of the surrounding medium. Hughes and Dowling[25] and Eldredge and Dowling[26] collectively verified Howe's model for $2.18 \times 10^{-4} \le d/\lambda \le 0.016$, $0.02 \le \beta \le 0.11$, and $0 \le M_2 \le 0.09$. The transmission loss of the perforated screen with bias flow is determined from Eq. (2)

$$L_T = -20\log_{10}(T_c). \quad (7)$$

Jing and Sun[10] investigated the effect of plate thickness on the acoustic impedance of perforated plates with bias flow. The authors re-expressed Howe's Rayleigh conductivity model [Eq. (5)] as the normalized acoustic impedance. An additional reactance term was included to account for plate thickness, resulting in the following expression:

$$z = \left(\frac{\pi ka}{2\beta}\right)\left(\frac{\delta_R}{\gamma_R^2 + \delta_R^2} - i\frac{\gamma_R}{\gamma_R^2 + \delta_R^2}\right) + i\frac{kl}{\beta}. \quad (8)$$

Equation (8) was experimentally validated[10] for $0.0129 \le \beta \le 0.0254$, $0.0027 \le d/\lambda \le 0.011$, and $0 \le M_2 \le 0.08$. Jing and Sun's experimental measurements and model predicted an increase in absorption with increasing plate thickness.

Betts[27] modified Crandall's impedance model[16] to account for high Mach number bias flow. Betts obtained an expression for the normalized perforation impedance

$$\begin{aligned} z = {} & \frac{16\nu l}{c\beta C_D d^2} + 2.82\frac{\sqrt{\omega\nu}}{c\beta C_D}\frac{l}{d} + \cdots \\ & + \frac{\rho}{\rho_2}\frac{(1-\beta^2)}{2c(\beta C_D)^2}[2u_b + 1.2u_{rms}] + \cdots \\ & + i\left(\frac{\omega l}{c\beta C_D} + 2.82\frac{\sqrt{\omega\nu}}{c\beta C_D}\frac{l}{d} + \frac{8d}{3\pi\psi(\beta)}\right), \end{aligned} \quad (9)$$

where ρ, c, ν, u_b, and u_{rms} are the density, propagation speed, kinematic viscosity of air, bias flow and root mean square (rms) velocity, respectively, upstream of the plate. The rms velocity was estimated using Eq. (4). Betts assumed a constant value for the discharge coefficient, $C_D = 0.76$, and used the inverse of Fok's function $\psi(\beta)$ to model interaction effects between perforations. Experimental validation was provided for $0.0007 \le d/\lambda \le 0.0129$, $0.059 < \beta < 0.165$, and $0.00221 \le M_2 \le 0.357$.

The impedance models proposed by Jing and Sun[10] and Betts[27] can be rewritten as an expression for transmission loss by examining the classic problem of acoustic wave transmission between two semi-infinite fluid media: one defined by the characteristic impedance of the air upstream of the perforated plate, and the other by the perforation impedance. The resultant expression is

$$L_T = -10\log_{10}\left(1 - \left|\frac{Z - \rho c}{Z + \rho c}\right|^2\right), \quad (10)$$

where ρc is the characteristic impedance upstream of the plate, and $Z = z\rho_2 c_2$ is the perforation impedance. Equations (7) and (10) are equivalent expressions for the insertion loss [Eq. (3)], since no wave reflection is implied by the absence of boundaries in the semi-infinite fluid media both upstream and downstream of the plate.

The assumptions and applicability of existing models[9,10,27] are now summarized to provide guidance for the proposed model in this work. Howe[9] and Jing and Sun[10] focused on low porosity plates so that acoustic interactions between the perforations can be ignored. Both analyses assumed negligible changes in the mean flow density, therefore validating the respective models for only small bias flow Mach number. Mass end correction and the *vena contracta* effect were not included in these investigations.[9,10] Betts' model accounted for HIE and was validated for high subsonic bias flow Mach numbers and higher porosity,[27] however, the range of validity is still restricted to porosity values less than those employed on bleed valve silencers.[15] The jet *vena contracta* was included in his analysis through the discharge coefficient, which was assumed constant.

C. Proposed model

We propose a model that is applicable over a larger range of porosity, acoustic frequencies, and bias flow Mach number than previous investigations.[9,10,27] For the perforation geometry and exit Mach number of the bleed-valve muffler,[15] hole interaction effects and mean flow compressibility must be included in the model. The *vena contracta* location is used to modify the static (zero bias flow) mass end correction.[18] Similar to the analysis of Betts[27] and Durrieu *et al.*,[8] the discharge coefficient is used to model hydrodynamic losses associated with mean flow separation and mixing downstream of the perforations. We include additional dependence of the discharge coefficient on the bias flow speed, porosity, plate thickness, and perforation diameter. The acoustic energy dissipation associated with vortical mixing downstream of the perforations is modeled by entropy fluctuations,[2] which are then used to modify the acoustic pressure transmitted downstream of the perforated plate.

The model is based on the work of Durrieu *et al.*[8] and Hofmans *et al.*[7] with modifications to the mass end correction and discharge coefficient for hole interaction effects and mean flow. The perforated plate is modeled as a duct containing a single contraction chamber with mean flow along the duct axis as shown in Fig. 2(a). The subscripts 1, 2′, *m*, and 3 refer to regions upstream of the contraction, within contraction, the *vena contracta* location, the mixing region downstream of the contraction, and the fully mixed region, respectively. The contraction is a discontinuous change in area at $x = 0$, and the ratio of contracted area to upstream area is defined by the porosity $\beta = A_{2'}/A_1$. The contraction expands discontinuously at $x = l$ to the original duct area $A_3 = A_1$. The Reynolds number $(u_{2'}d/\nu_{2'})$ in the contraction is assumed sufficiently large so that viscosity has the sole effect of flow separation at the upstream

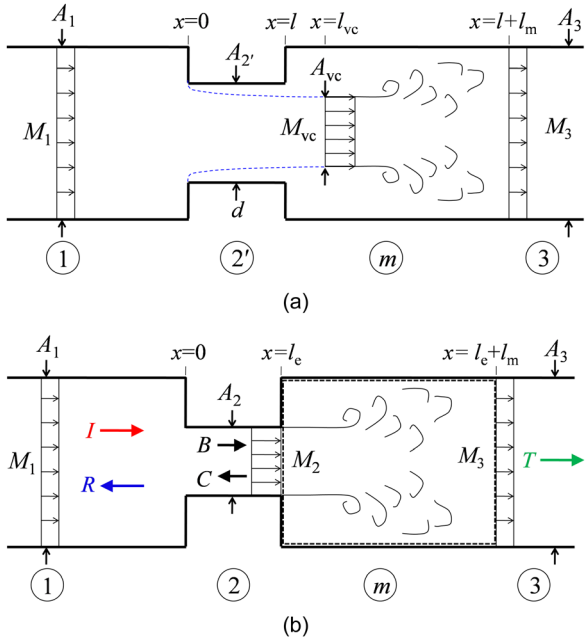

FIG. 2. (Color online) Contraction chamber used for one-dimensional modeling of perforated plate acoustics with bias flow. (a) Contraction area corresponds to actual perforation diameter and the dashed line represents the separation streamline of the free jet. (b) Contraction area is equal to the *vena contracta* area, and the control volume (dashed line) encloses the mixing region downstream of the expansion plane.

corner of the contraction, as illustrated by the dashed lines in Fig. 2(a). A free jet forms downstream of the contraction plane ($x=0$), contracting to a minimum area A_{vc} at the *vena contracta* ($x=l_{vc}$). At the *vena contracta*, the density, pressure, and Mach number M are approximately uniform. Irreversible losses that occur in the mixing region downstream of the *vena contracta* are represented in this study through fluctuations in entropy. After a distance l_m downstream from the expansion, the acoustic and mean flow properties are approximately one-dimensional in region 3.

In the following analysis, the mean flow in region 2′ is approximated as one-dimensional and parallel to the duct axis. The change in mean flow speed is discontinuous at $x=0$, and the separation of the jet and its profile are modeled as a contraction of constant area, equal to the *vena contracta* area [Fig. 2(b), region 2]. The jet Mach number M_2 is subsonic, and the acoustic wavelength is assumed much larger than the contraction diameter. This allows the approximation of one-dimensional acoustic wave propagation in regions 1, 2, and 3 of the duct. The contraction length is corrected using an effective length, l_e, that accounts for hole interaction effects and bias flow.

The acceleration of the mean flow between regions 1 and 2 is assumed inviscid and isentopic. The following integral forms for conservation of mass and energy apply, along with the isentropic relation:

$$\rho_1 u_1 = \rho_2 u_2 \beta C_c, \tag{11}$$

$$\frac{\gamma}{\gamma-1}\frac{p_1}{\rho_1}+\frac{u_1^2}{2}=\frac{\gamma}{\gamma-1}\frac{p_2}{\rho_2}+\frac{u_2^2}{2}, \tag{12}$$

$$\frac{p_1}{\rho_1^\gamma}=\frac{p_2}{\rho_2^\gamma}. \tag{13}$$

Equation (11) implies that the *vena contracta* area $A_{vc}=A_2=A_1\beta C_c$, where C_c is the area contraction coefficient. Downstream of the duct expansion, the conservation equations are applied to the control volume illustrated in Fig. 2(b) as the dashed line. The left surface of the control volume is located at $x=l$, the top and bottom surfaces are coincident with the walls of the duct, and the right surface is located at length $x=l_e+l_m$ that is sufficiently downstream of the expansion so that the jet is completely mixed and the flow properties are uniform along this surface. Mass conservation between the left ($x=l$) and right ($x=l+l_m$) surfaces of the control volume requires that

$$\rho_2 u_2 \beta C_c = \rho_3 u_3. \tag{14}$$

Assuming that the flow expands adiabatically

$$\frac{\gamma}{\gamma-1}\frac{p_2}{\rho_2}+\frac{u_2^2}{2}=\frac{\gamma}{\gamma-1}\frac{p_3}{\rho_3}+\frac{u_3^2}{2}. \tag{15}$$

Neglecting friction along the walls of the duct, the axial momentum conservation at the left and right surfaces of the control volume reduces to

$$p_2+\rho_2 u_2^2 \beta C_c = p_3+\rho_3 u_3^2. \tag{16}$$

The contraction coefficient C_c in Eqs. (11), (14), and (16) is determined using the discharge coefficient $C_c=C_D/0.98$, where 0.98 is the velocity coefficient for a free jet leaving a sharp-edged orifice.[28] The discharge coefficient C_D is determined based on an empirical correlation formula provided by Smith and Van Winkle[29] for perforated plates

$$C_D = K\left(\frac{d}{P}\right)^{0.10}, \tag{17}$$

where K is specified by the Reynolds number in the contraction, $\mathrm{Re}_2=u_2 d/\nu_2$, and l/d, using Fig. 9 from Ref. 27. The distance between perforations, P, is determined based on the pattern of the perforation grating. For a rectilinear pattern, P is defined as[30]

$$P = 0.89\frac{d}{\sqrt{\beta}} \tag{18}$$

and for a triangular pattern

$$P = 0.9498\frac{d}{\sqrt{\beta}}. \tag{19}$$

Equations (11)–(16) define the mean flow properties throughout the entire domain. Assuming time harmonic disturbances of the exponential form $e^{i\omega t}$, where $\omega=2\pi f$ is the angular frequency, the acoustic pressure throughout the domain in Fig. 2(b) can be expressed as

$$
\begin{aligned}
p'(x,t) &= Ie^{i(\omega t-[(kx)/(1+M_1)])} + Re^{i(\omega t-[(kx)/(1-M_1)])}; \quad x<0\\
p'(x,t) &= Be^{i(\omega t-[(kx)/(1+M_2)])} + Ce^{i(\omega t-[(kx)/(1-M_2)])}; \quad 0\le x\le l_e\\
p'(x,t) &= Te^{i(\omega t-[(kx)/(1+M_3)])}; \quad x>l_e+l_m.
\end{aligned}
\tag{20}
$$

For one-dimensional, isentropic wave propagation, the relations between velocity and density fluctuations to pressure fluctuations are

$$u' = \frac{\pm p'}{\rho c}, \tag{21}$$

$$\rho' = \frac{p'}{c^2}. \tag{22}$$

Equation (22) is applicable where the mean flow is isentropic. Irreversible flow losses occur due to mixing and viscous dissipation as the flow develops downstream of the contraction (Fig. 2). The losses associated with the flow in the mixing region produce fluctuations in entropy that propagate downstream at the mean flow velocity in region 3. The acoustic density fluctuations in region 3 are expressed as pressure and entropy fluctuations[2]

$$\rho_3' = \frac{\rho_3'}{c_3^2} - \frac{\bar{\rho}_3\bar{T}_3(\gamma-1)s_3'}{c_3^2}, \tag{23}$$

where the overbar and $()'$ indicate the mean and perturbed quantity, respectively. The second term on the right-hand side of Eq. (23) indicates a perturbation from the isentropic relation defined in Eq. (22). Equation (23) can be rewritten in the form

$$\rho_3' = \frac{p_3' + \delta}{c_3^2}, \tag{24}$$

where δ is a correction to the pressure fluctuations in region 3 that accounts for dissipation of acoustic energy in the mixing region. The mean flow process in region 3 is inviscid and adiabatic, and therefore the mean entropy associated with a fluid particle in this region remains constant, or $Ds/Dt = 0$. Here, $D/Dt = \partial/\partial t + u\partial/\partial x$ is the convective derivative, and the entropy fluctuations in region 3 propagate at speeds associated with the local mean flow, u_3. The entropy fluctuations are not directly involved in the generation of true sound because acoustic fluctuations propagate at speeds corresponding to the sound velocity.[31]

Phong and Papamoschou[1] showed that the end effects associated with the acoustic radiation from open ended tubes are an essential component in modeling the transmission behavior of perforated plates without bias flow. The end correction included interactions between the perforations in the form of a correction to the physical thickness of the plate. The thickness correction, l', was defined as

$$l' = \frac{8d}{3\pi\psi(\beta)}, \tag{25}$$

where $\psi(\beta)$ is a function derived by Fok that describes the acoustic interactions between the perforations.[19] Equation (25) was found to be accurate in describing the static transmission behavior of a perforated plate,[1] and consequently must be modified to include the effect of bias flow. Fok's function[19] was derived based on potential theory, and therefore Eq. (25) is applicable only where the mean flow is irrotational. Melling[32] proposed a qualitative explanation of the effect of bias flow on the end correction associated with perforated plates: "up to the *vena contracta*… the mass reactance due to the attached mass is presumed to exist and beyond this point is destroyed." The attached mass is modified in this study by using the *vena contracta* location of the jet. Figure 3 schematically illustrates this modification for a single perforation.

The *vena contracta* length, l_{vc}, is defined in the present work as the distance between the upstream surface of the plate and the *vena contracta* location. The *vena contracta* location is approximated from the jet profile computed by Rouse and Abul-Fetouh.[33] From their results, the jet diameter contracts to within 1% of its fully contracted value at $x/a = 1.4$, and therefore the *vena contracta* location is approximated at $l_{vc} = 1.4a$ in this work. Observing Fig. 3, the effective length l_e, or sum of the plate thickness and end correction length, is defined by three cases:

$$
\begin{aligned}
l_e &= l + l'; \quad l_{vc} > l'/2\\
l_e &= l'/2 + l_{vc}; \quad l < l_{vc} < l'/2\\
l_e &= l + l'/2; \quad l_{vc} < l.
\end{aligned}
\tag{26}
$$

The first condition ($l_{vc} > l'/2$) in Eq. (26) implies that the end correction length for perforations with bias flow cannot exceed the static end correction [Eq. (25)]. The second condition ($l < l_{vc} < l'/2$) follows Melling's assumption: the end correction length on the downstream side of the plate (see

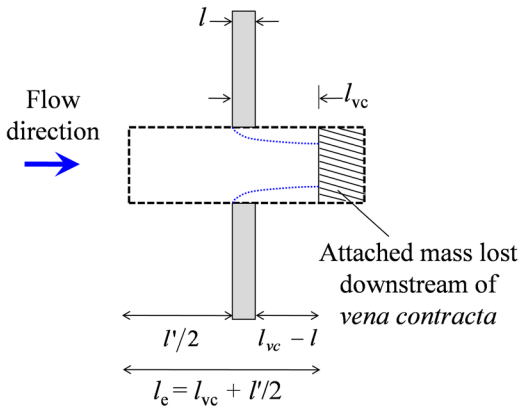

FIG. 3. (Color online) End correction associated with a single orifice, showing modification for bias flow. Dashed line indicates the idealized attached mass with total length l' determined by potential theory (see Ref. 18) for the zero bias flow case. Shaded region represents length reduction due to mixing downstream of the *vena contracta*.

Fig. 3) cannot exceed the *vena contracta* location. The third condition ($l_{vc} < l$) assumes that significant mixing does not occur until the flow leaves the perforations, and therefore the mean flow is approximately potential everywhere inside the perforation.

Applying acoustic perturbations to p, ρ and u, and linearizing Eqs. (11), (12), (14), (15), and (16) results in the following set of equations:

$$\frac{\beta C_c}{c_2}\left[(1+M_2)Be^{-ik_2^+ l_e} - (1-M_2)Ce^{ik_2^- l_e}\right] = \frac{1}{c_3}\left[(1+M_3)Te^{-ik_3^+(l_e+l_m)} + M_3\delta e^{-ik_\sigma^+(l_e+l_m)}\right], \quad (27)$$

$$\frac{1}{c_1}[(1+M_1)I - (1-M_1)R] = \frac{C_c\beta}{c_2}[(1+M_2)B - (1-M_2)C], \quad (28)$$

$$[\beta C_c(M_2^2+2M_2)+1]Be^{-ik_2^+ l_e} + \cdots + [\beta C_c(M_2^2-2M_2+1)]Ce^{ik_2^- l_e} = (1+M_3)^2 Te^{-ik_3^+(l_e+l_m)} + M_3^2\delta e^{-ik_\sigma^+(l_e+l_m)}, \quad (29)$$

$$\frac{1}{\bar{\rho}_2}\left[(1+M_2)Be^{-ik_2^+ l_e} + (1-M_2)Ce^{ik_2^- l_e}\right] = \frac{1}{\bar{\rho}_3}\left[(1+M_3)Te^{-ik_3^+(l_e+l_m)} - \frac{\delta}{\gamma-1}e^{-ik_\sigma^+(l_e+l_m)}\right], \quad (30)$$

$$\frac{1}{\bar{\rho}_1}[(1+M_1)I + (1-M_1)R] = \frac{1}{\bar{\rho}_2}[(1+M_2)B + (1-M_2)C]. \quad (31)$$

Equations (27)–(31) are a linear system of equations in which the transmitted wave amplitude T can be computed if the incident wave amplitude I is specified. The acoustic energy flux of a plane wave propagating along the same direction as a medium in motion is expressed as[17]

$$J = \frac{1}{\bar{\rho}c}\left[(1+M)^2\langle p'^2\rangle\right], \quad (32)$$

where the angle brackets denote time averaging. The acoustic power is determined by multiplying Eq. (32) by the appropriate duct area. Since $A_1 = A_3$, the transmission loss is determined from Eq. (2)

$$L_T = 10\log_{10}\left(\frac{\bar{\rho}_3 c_3}{\bar{\rho}_1 c_1}\frac{(1+M_1)^2}{(1+M_3)^2}\frac{|I|^2}{|T|^2}\right). \quad (33)$$

In the absence of an area contraction and viscosity, the incident wave in region 1 propagates downstream to region 3 without any loss in power. This means that $\Pi_i = \Pi_{t,0}$, where $\Pi_{t,0}$ is the sound power of the transmitted wave in region 3, without the duct contraction. Comparing Eqs. (2) and (3), the transmission loss [Eq. (33)] is an equivalent expression for the insertion loss ($L_T = L_I$) under the approximations of the proposed model.

III. EXPERIMENTAL SETUP

A special facility was designed and built for the measurement of insertion loss of perforated plates at normal incidence and with bias flow. The facility comprised three sections, as shown in Fig. 4. The first section conditioned the air flow supply, which was injected radially through ports at the upstream end of the apparatus. Turbulence was suppressed using a 0.32-cm cell size honeycomb, followed by a series of screens. The second section of the facility contained the acoustic source. Here, an impinging jets setup[34] was used to simulate a broadband monopole-type noise source. The impinging jets were supplied at a pressure 517 kPa by four 1.6 mm internal diameter tubes, resulting in a net mass flow rate $\dot{m} = 9.81 \times 10^{-4}$ kg s^{-1}. A bell-shaped convergent section at the end of the source section ensured uniform axial flow at the sample mounting plate. The convergent section was 20.7 cm in length and had an area contraction ratio of 16.8, resulting in a contraction diameter of 4.57 cm immediately upstream of the sample mounting plate. The sample mounting plate had a 4.57 cm diameter hole bored in its center that allowed airflow through from the convergent section. The perforated plates were mounted on the downstream surface of the sample mounting plate over the center-bored

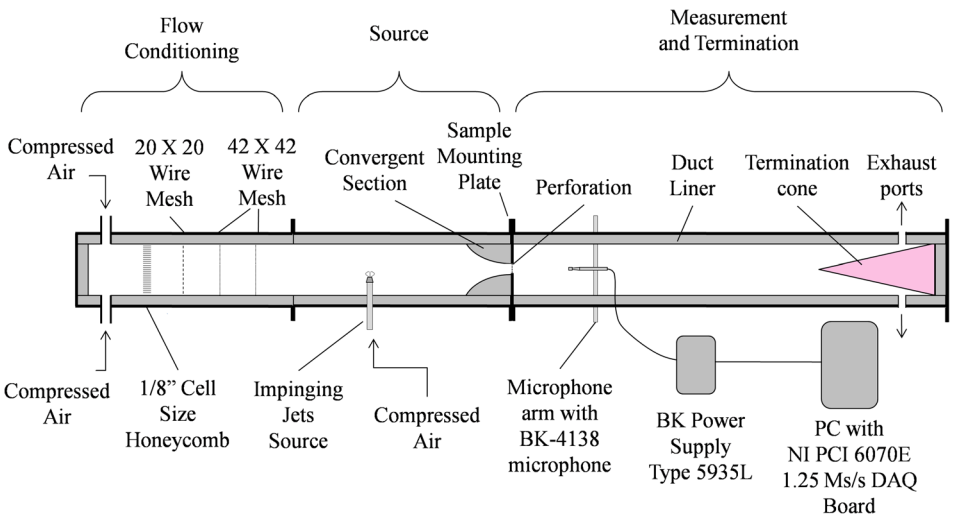

FIG. 4. (Color online) Schematic of experimental facility.

hole. The third section contained the acoustic measurement apparatus and anechoic termination. A 3.2 mm condenser microphone (model 4138, Brüel & Kjaer, Nærum, Denmark) with a frequency response of 140 kHz was mounted on a traversable arm downstream of the sample. The microphone orientation was parallel to the duct axis and against the flow. To prevent reflections from the end of the measurement section, a sound absorbing cone was installed. Internal reflections from the duct walls were minimized by installing 3.8 cm duct liner (SoundVAC) in all sections. The effective internal diameter of all sections was 18.73 cm after installation of the liner.

Figures 5(a) and 5(b) detail the acoustic measurement setup downstream of the perforated plate. The local sound intensity was computed based on SPL measurements at 19 radial locations, each separated by 6.4 mm, along the measurement plane [Fig. 5(b)]. An additional apparatus which secured the microphone to the traversable arm introduced a 12.7 mm offset of the measurement axis from the duct center. The traversable arm was centered for structural considerations and to maximize the spatial range of the microphone. The sound power in the duct was estimated by spatially averaging the sound intensity measurements over areas, dA, associated with the 19 measurement positions (Table I). An aerodynamic forebody (G.R.A.S. Model RA0173) was attached to the microphone, effectively suppressing flow induced noise[35] for mean flow velocity up to 20 m/s. The microphone was connected to a dual channel power supply/conditioning amplifier (type 5935L, Brüel & Kjaer). The output of the signal was sampled at 250 kS/s by a multifunction data acquisition board (PCI-6070E, National Instruments, Austin, TX) installed in a Dell Optiplex 380 personal computer with an Intel Core 2 Duo processor. National Instruments LabView software was used to acquire the microphone signal. The resultant signal was conditioned with a high-pass filter set at 350 Hz. The narrowband spectra were computed using a 4096-point ($\Delta f = 61$ Hz) Fast Fourier Transform and were corrected for microphone frequency response, free-field response, atmospheric absorption and the aerodynamic forebody.

TABLE I. Radii, incidence angle from duct centerline, and associated area for measurement positions 1 through 19.

n	r_n	θ_n	dA_n
1	58.983	17.68	1185.9
2	52.751	15.72	1060.6
3	46.565	13.80	936.3
4	40.446	11.93	813.2
5	34.428	10.11	692.2
6	28.577	8.37	574.6
7	23.020	6.73	462.8
8	18.031	5.26	362.5
9	14.221	4.14	285.9
10	12.7	3.70	255.3
11	14.221	4.14	285.9
12	18.031	5.26	362.5
13	23.020	6.73	462.8
14	28.577	8.37	574.6
15	34.428	10.11	692.2
16	40.446	11.93	813.2
17	46.565	13.80	936.3
18	52.751	15.72	1060.6
19	58.983	17.68	1185.9

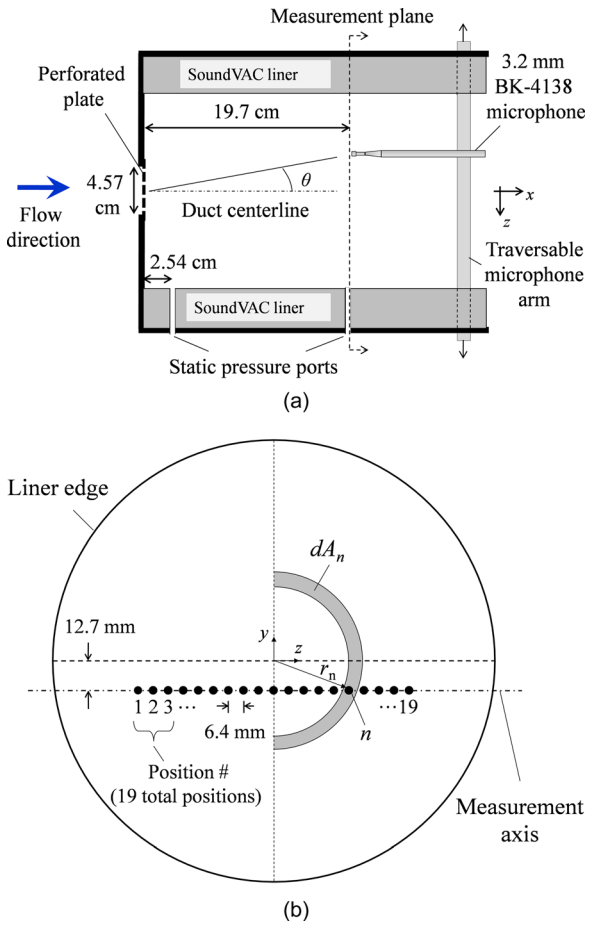

FIG. 5. (Color online) Acoustic measurement setup downstream of perforated plate, showing (a) microphone and static pressure port positions relative to the perforated plate and (b) spatial locations and associated areas used to calculate sound power at the measurement plane.

The acoustic intensity level for a plane wave in a non-stationary medium is related to the sound pressure by the following expression:

$$\mathrm{IL}_n = 10\log_{10}\left[(1+M_n)^2\frac{p_n'^2}{\rho c I_{\mathrm{ref}}}\right]. \tag{34}$$

Here n is the index corresponding to the measurement position in Fig. 5(b), M_n is the Mach number, and $I_{\mathrm{ref}} = 10^{-12}\,\mathrm{W\,m^{-2}}$ is the reference intensity. The intensity was assumed constant over the strip of area, dA_n, where $dA_n = 0.5\pi\ [(r_n+3.2)^2 - (r_n-3.2)^2]$. M_n was determined from Pitot pressure measurements of the flow field downstream of the perforated plate and wall static pressure measurements on the measurement plane [Fig. 5(a)]. The Mach number at the measurement plane did not exceed 0.06 for all plates. Therefore, variations in mean density and temperature did not exceed 0.2% and 0.1%, respectively, from their static values and the approximation $p^2_{\mathrm{ref}} = \rho c I_{\mathrm{ref}}$ holds satisfactorily, where $p_{\mathrm{ref}} = 20\,\mu\mathrm{Pa}$. The acoustic intensity level spectrum recasted in terms of SPL is

$$\mathrm{IL}_n(f) = 10\log_{10}[(1+M_n)^2 10^{0.1\mathrm{SPL}_n(f)}]. \quad (35)$$

The sound power level (PL) is determined assuming the local intensity level spectrum is constant over the respective area dA_n

$$\mathrm{PL}_{\exp}(f) = \sum_{n=1}^{19} \mathrm{IL}_n(f) dA_n. \quad (36)$$

The insertion loss (L_I) was measured based on the difference in the PL spectrum with and without (baseline case) the perforated plate attached to the sample mounting plate

$$L_{I,\exp}(f) = \mathrm{PL}_{0,\exp}(f) - \mathrm{PL}_{\exp}(f). \quad (37)$$

A total of 12 experimental cases were tested: the baseline case (denoted with a "0" subscript) where no perforation is installed, and 11 different perforated plates. The key parameters of each perforated plate used in the experiments are summarized in Table II. The samples tested in this study are identical to those used previously for static insertion loss measurements (Ref. 1), to isolate the effect of flow through the perforations. The insertion loss was measured over a range of $0 \le M_1 \le 0.1$. For $M_1 > 0.06$, total pressure measurements at the measurement plane of the duct indicated that the local mean flow velocity exceeded 20 m/s, the limit beyond which suppression of flow noise by the microphone forebody cannot be guaranteed.[35] Therefore, only results for $0 \le M_1 \le 0.06$ are presented in this work. The corresponding range of Mach number through the perforation is $0 \le M_2 \le 0.25$.

IV. RESULTS

A. Robustness of setup

As described in Sec. III, an in-duct method was used to determine the total power of the acoustic wave at the measurement plane of the duct. In addition to sound pressure fluctuations from the source, the microphone measures turbulent pressure fluctuations associated with the mean flow.[36] The model proposed in Sec. II C [Eq. (33)] does not include noise generation associated with fluctuations from the flow; therefore, it was necessary to discriminate between pressure fluctuations from the impinging jets source and the mean flow. This was accomplished by examining the signal-to-noise ratio (SNR), where the desired signal is composed of fluctuations from the impinging jets source only.

TABLE II. Properties of perforated sheets used in experiments.

Plate	Porosity β	Thickness l (mm)	Hole diameter d (mm)	Hole spacing P (mm)	Perforation grating
—	1.00	—	—	—	—
1	0.37	0.6096	1.1430	1.676	Square
2	0.48	0.4064	2.6162	3.353	Square
3	0.37	0.4064	1.1430	1.676	Square
4	0.29	0.4064	1.0160	1.676	Square
5	0.45	0.7620	1.7526	2.794	Triangular
6	0.23	0.7620	1.5875	3.175	Triangular
7	0.23	0.9144	1.5875	3.175	Triangular
8	0.23	0.4064	0.6858	1.270	Square
9	0.23	0.4064	0.6096	1.118	Square
10	0.22	0.4064	0.5080	1.016	Triangular
11	0.22	0.4064	0.4064	0.889	Triangular

The SNR was determined by comparing the PL spectra between two run conditions. First, the power level spectrum was measured with the impinging jets source and mean flow both in operation. Next the power level spectrum was measured with only the mean flow in operation, therefore isolating the spectral content associated with the flow noise. Assuming that the sound from the impinging-jets source and flow noise sources are uncorrelated, the SNR is defined as

$$\mathrm{SNR}_{\mathrm{dB}}(f) = 10\log_{10}\left(\frac{\mathrm{PL}_{\mathrm{signal}}(f)}{\mathrm{PL}_{\mathrm{noise}}(f)}\right), \quad (38)$$

where $\mathrm{PL}_{\mathrm{signal}}$ and $\mathrm{PL}_{\mathrm{noise}}$ are the PL of the impinging-jets source and flow noise, respectively. Figure 6 compares the power level spectra of pressure fluctuations from both mean flow and the impinging jets source, with the spectra of fluctuations associated with only the mean flow for plate 1. The solid and dotted lines are measurements at $M_1 = 0.02$ and 0.06, respectively. Comparing the noise floor (both mean flow and the impinging jets source not in operation) and flow noise spectra, Fig. 6 indicates that the spectral content of flow noise is predominantly low-frequency; however, at larger bias flow speeds, the flow noise also contains broadband high frequency content. The extent to which low frequencies are contaminated by flow noise increases as the bias flow Mach number increases. At higher frequencies, there is a large separation in the power level spectra between the two run conditions. Similar SNRs were obtained for plates 2–11, indicating signal contamination at low frequencies due to flow noise. Existing literature on in-duct acoustic measurements[36,37] recommends a minimum SNR of 6 dB to ensure accurate data recovery of an acquired signal. Therefore, only frequency components of the PL spectrum where the SNR $\ge$ 6 dB were considered valid measurements of insertion loss.

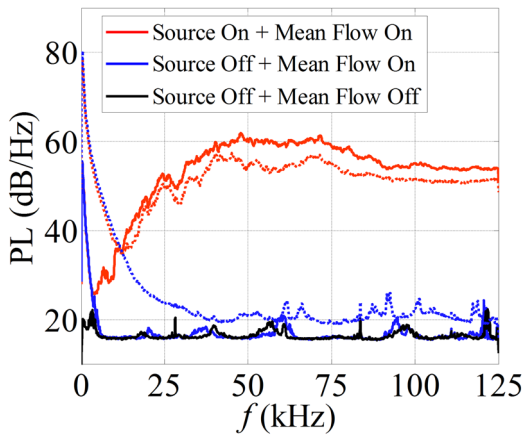

FIG. 6. (Color online) PL spectra of flow conditions corresponding to both source and mean flow in operation, only mean flow in operation, and background noise for plate 1. Solid and dashed lines are spectra for $M_1 = 0.02$ and $M_1 = 0.06$, respectively.

B. Insertion loss

Figures 7(a)–7(d) compare the insertion loss predictions of Eq. (33) with experimental measurements of this study. Plates 1, 2, 6, and 11 are selected as representative cases that cover the range of porosity, hole diameter, and plate thickness used in the experiment. The insertion loss is plotted versus d/λ to facilitate the explanation of discrepancies between Eq. (33) and experiment. Comparisons between the dotted and solid lines in Figs. 7(a)–7(d) for $M_1 = 0$ indicate good agreement between Eq. (33) and measured insertion loss in the absence of bias flow. For all plates, Eq. (33) predicts a decrease in L_I to zero for $M_1 = 0$ as d/λ decreases, a trend clearly seen in the experimental data. As d/λ increases, Fig. 7(c) indicates a saturation followed by decline of insertion loss. The saturation is caused by standing-wave-formed resonances inside the contraction as the acoustic wavelength approaches the order of the plate thickness l. It is analogous to Fabry-Pérot-type resonance observed in optics.[22,23] Figure 7(c) indicates that Eq. (33) predicts accurately the frequency corresponding to peak insertion loss measured in the experiments. The maximum resolvable frequency in this study corresponded to an acoustic wavelength that exceeds resonant conditions for thin plates [Figs. 7(b) and 7(d)]. Therefore, only the initial increase in insertion loss is resolved in Figs. 7(b) and 7(d). The insertion loss would expectedly peak and decline as the acoustic frequency further increases. Figure 7(c) indicates a significant departure between experiment and theory at wavelengths equal to or greater than the spacing between perforations ($P/\lambda \geq 1$ or $d/\lambda \geq 0.5$). Previous investigations noted "extraordinary" transmission behavior, similar to Wood's anomaly,[21–23] when the wavelength becomes similar to the perforation spacing. Table III lists the maximum dimensionless length scale, P/λ, resolved for all plates tested in this study. Here, plates 2, 5, 6, and 7 have sufficient perforation spacing to satisfy $P/\lambda > 1$, and may be impacted by Wood's anomaly over the experimental frequency range.

The deviations observed in Fig. 7(b) at $d/\lambda > 0.6$ for plate 2 is attributed to non-planar modes of acoustic wave propagation. A circular duct containing one-dimensional, inviscid, axial mean flow will contain non-planar acoustic modes under the following condition:[17]

$$\frac{d}{\lambda} > \frac{\mu_{kj}}{\pi}\sqrt{1 - M^2}. \tag{39}$$

Here M is the bias flow Mach number in the perforation and μ_{kj} is the jth zero of the first derivative of the kth-order Bessel function of the first kind $[J'_k(\mu_{kj}) = 0]$. The first non-planar mode is cut-on when $(k,j) = (1,0)$, or when $\mu_{10} = 1.84$. This means that the one-dimensional assumption of our model breaks down for $d/\lambda > 0.586$ or lower, depending on the bias flow Mach number in the perforation.[17] The maximum d/λ resolved for all perforations tested in this study is listed in Table III. Except for plates 2 and 5, the perforation diameter of the remaining plates cannot sustain non-planar modes at the highest resolved acoustic frequency. Since Eq. (39) is satisfied for plates 2 and 5, the departure between Eq. (33) and

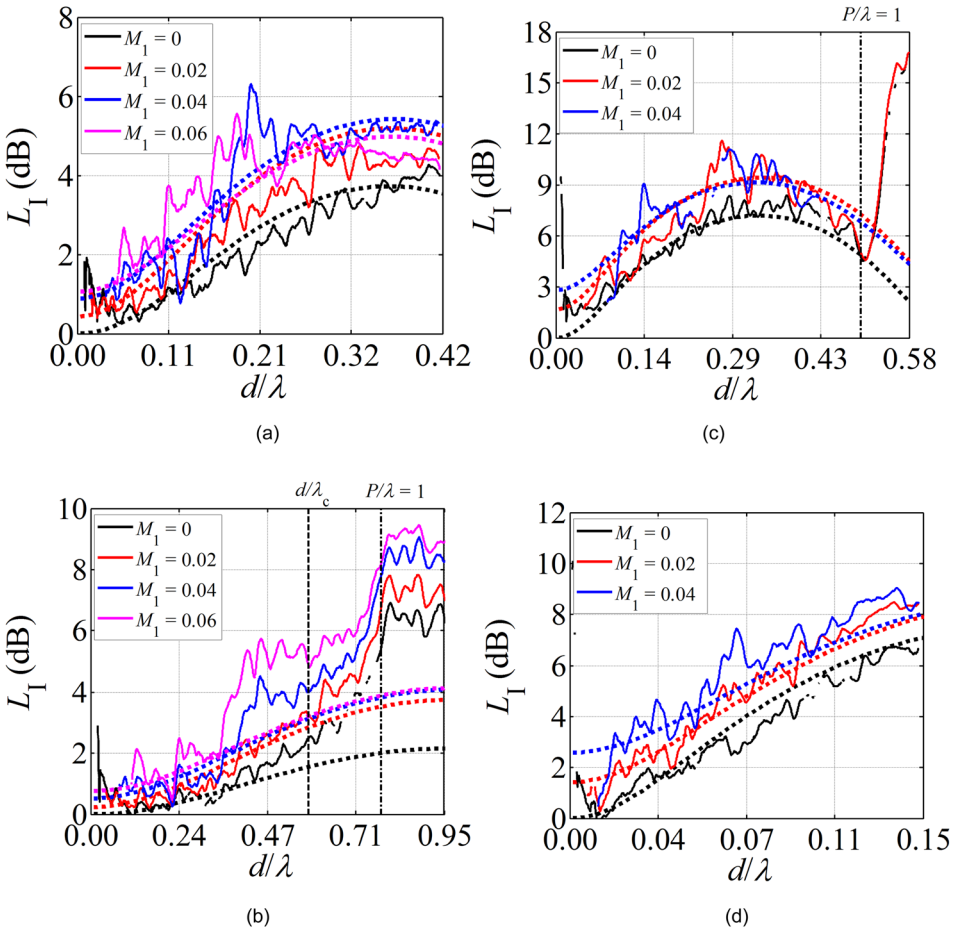

FIG. 7. (Color online) Insertion loss versus perforation hole diameter scaled by acoustic wavelength d/λ for (a) plate 1; (b) plate 2; (c) plate 6; and (d) plate 11. Solid and dotted lines indicate experiment measurements and Eq. (33), respectively. Vertical dashed line indicates minimum d/λ at which non-planar acoustic modes are cut-on. Vertical dash dotted line indicates the value of d/λ at which transmission behavior may be affected by Wood's anomaly (Refs. 21–23).

TABLE III. Maximum dimensionless hole diameter, and dimensionless hole spacing resolved in experiments.

Plate	$d/\lambda\|_{max}$	$P/\lambda\|_{max}$	d/λ at $P/\lambda = 1$
1	0.417	0.611	—
2	0.953	1.222	0.780
3	0.417	0.611	—
4	0.370	0.611	—
5	0.639	1.018	0.627
6	0.579	1.157	0.500
7	0.579	1.157	0.500
8	0.250	0.463	—
9	0.222	0.407	—
10	0.185	0.370	—
11	0.148	0.324	—

measurements in Fig. 7(b) for $d/\lambda > 0.6$ is attributed to propagating non-planar modes.

At bias flow Mach number $0.04 \le M_1 \le 0.06$, additional losses are observed for plates 1 and 2 [Figs. 7(a) and 7(b)], at acoustic frequencies smaller than the cut-on condition for non-planar modes [Eq. (39)]. The additional losses are due to errors inherent in the approximations made in determining the duct sound power. Table I indicates that dA_n is much larger at positions away from the duct center, therefore the PL calculation is area weighted with more bias near the duct wall. The microphone is more susceptible to transverse pressure fluctuations and cross flow as the incidence angle θ_n increases away from the duct centerline. Here, the acquired signal may become contaminated by flow induced resonance or cavity pressure oscillations produced locally at the microphone nosecone.[38] The error associated with near-wall measurements is more pronounced in the insertion loss spectrum due to the larger area weighting. As the bias flow Mach number increases, the experimental trends in Figs. 7(a)–7(d) and all remaining plates show an increase in insertion loss at small d/λ with increasing bias flow Mach number.

We now assess the validity range of Eq. (33) by comparing its predictions with the models of previous investigations.[9,10,27] Previous models were validated over the parameter space $0.001 \le d/\lambda \le 0.02$, and $0 \le M_2 \le 0.35$, and therefore fair comparisons can only be made within these ranges of d/λ and M_2. Because of a combination of flow induced noise and the perforation diameter sizes in this work, only plates 8–11 contain experimental measurements that satisfy the SNR criterion of Eq. (38) and fall within $0.001 \le d/\lambda \le 0.02$. Plates 10 and 11 (Figs. 8 and 9) are selected for comparison with previous models[9,10,27] with focus on the aforementioned parameter space. All the models predict an increasing insertion loss with

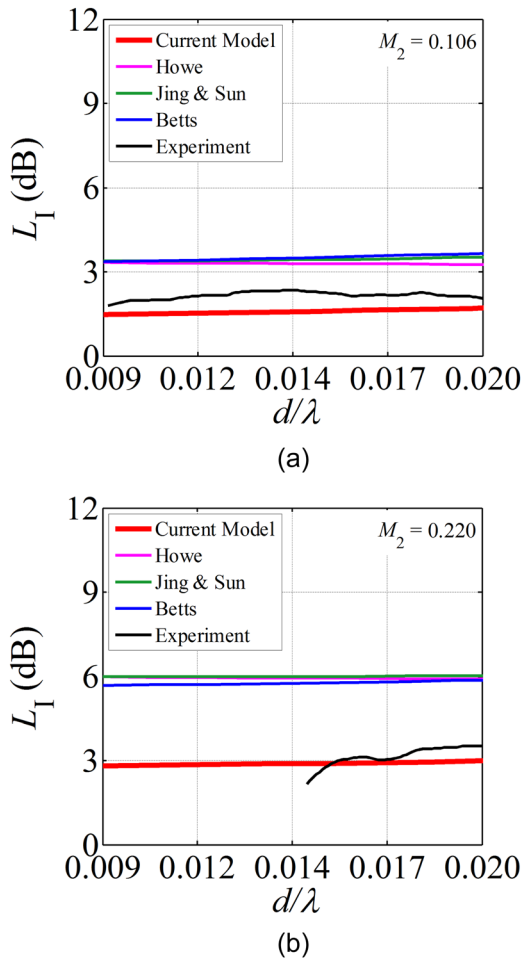

FIG. 8. (Color online) Comparison of insertion loss between experiment, proposed theoretical model Eq. (33), and previous models (see Refs. 9, 10, and 27) for plate 10 at (a) $M_2 = 0.106$; (b) $M_2 = 0.220$.

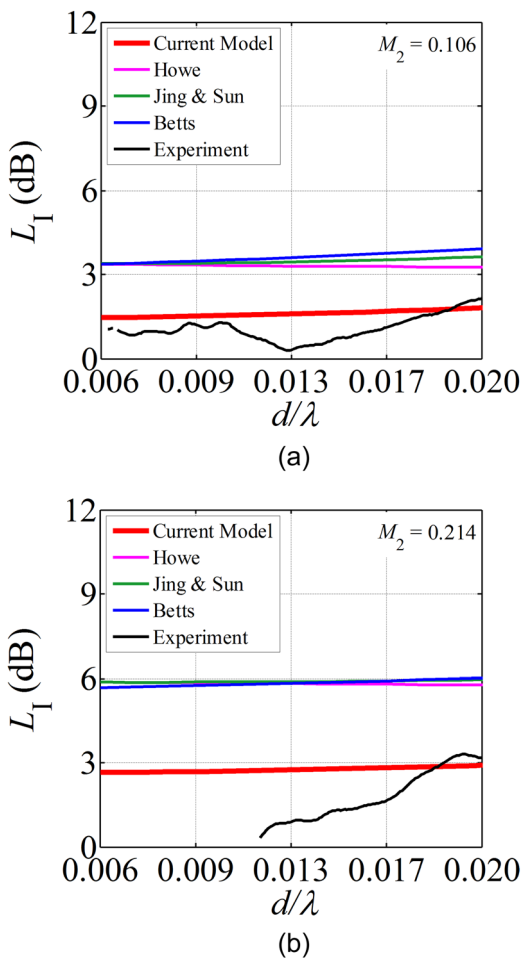

FIG. 9. (Color online) Comparison of insertion loss between experiment, proposed theoretical model Eq. (33), and previous models (see Refs. 9, 10, and 27) for plate 11 at (a) $M_2 = 0.106$; (b) $M_2 = 0.214$.

increasing d/λ and M_2. For the validated $d/\lambda \leq 0.02$, Eq. (33) yields more accurate predictions of insertion loss over previous models at $M_2 = 0.11$ [Figs. 8(a) and 9(a)]. Near $d/\lambda = 0.02$, the increase in L_I as M_2 increases to 0.2 is more accurately predicted by Eq. (33) than previous models [Figs. 8(b) and 9(b)]. The improvement in prediction by the present model underscores the advantage of using entropy fluctuations to model additional acoustic power losses due to bias flow for high frequency applications.

Figures 10(a) and 10(b) compare the predictions of Eq. (33) with those of previous models for plates 6 and 2, respectively, at values of d/λ up to 0.5. Although previous models lacked validation at high d/λ values, some key advantages of the current model over previous models are underscored at large d/λ for thick plates (plate 6) and large porosity (plate 2). Figure 10(a) indicates that all previous models[9,10,27] fail to resolve the saturation and decline of L_I, a result of standing-wave formed resonance as the acoustic wavelength approaches the thickness of the perforated plate. The failure to resolve this phenomenon results from the assumption that $kl \ll 1$. This condition implies negligible changes in pressure fluctuation phase and amplitude over the characteristic dimensions of the perforation, and is a requirement for lumped parameter models of acoustic filters.[17] Using the wave propagation speed $c = 343$ m/s, and the maximum acoustic frequency resolved in our experiments

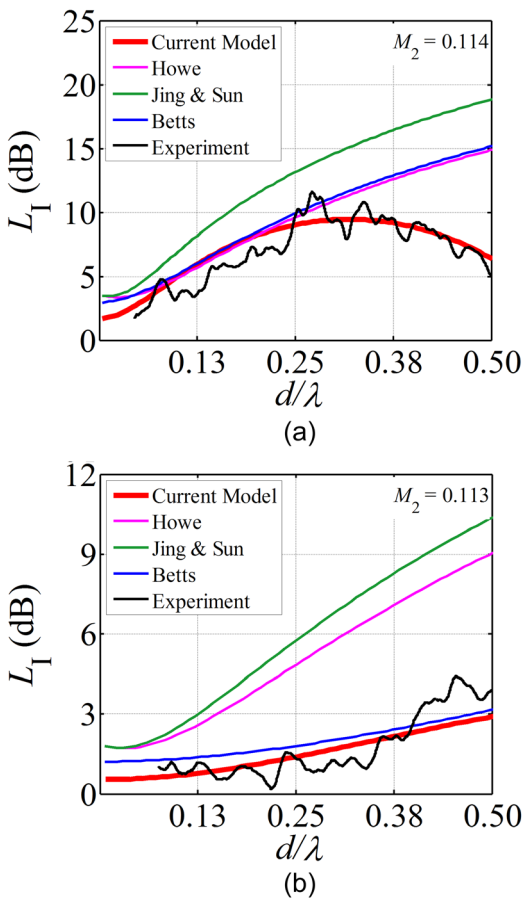

FIG. 10. (Color online) Comparison of insertion loss between experiment, proposed theoretical model Eq. (33), and previous models (see Refs. 9, 10, and 27) for (a) plate 6 at $M_2 = 0.114$; (b) plate 2 at $M_2 = 0.113$.

($f = 125$ kHz), a lumped parameter model requires $l \ll 0.437$ mm. The thickness of samples used in this study ranges between $0.4064 < l < 0.9144$ mm, indicating that lumped parameter modeling cannot be used for the applications considered here. Figure 10(b) evaluates the accuracy to which all models are capable of predicting insertion loss for plates of high porosity. A large discrepancy is noted between experimental measurements and Howe's model,[9] and can be explained by the assumption of no acoustic interactions between the perforations. Jing and Sun[10] modified Howe's model[9] with an impedance correction to include the effect of plate thickness. Their model[10] converges to Howe's model[9] at low d/λ, as the additional reactance term in Eq. (8) reduces to zero. At higher d/λ, the effect of thickness in Jing and Sun's model is to increase L_I, resulting in greater error relative to the current measurements. The authors had noted in their work[10] that the additional reactance term corresponding to the thickness correction in their model overestimated the reactance when compared to their experiments. They claimed that the reactance error was large at high bias flow speeds due to the effect of flow separation, which was not included in their model.[10]

Betts' impedance model[27] yields similar trends as the models of Howe[9] and Jing and Sun:[10] an increase in insertion loss over the entire range of d/λ with increasing bias flow Mach number. The trends in his model are consistent with the current experimental results; however, his model over predicts the insertion loss within the region of validated d/λ (Figs. 8 and 9). Betts' model is more accurate for plates of higher porosity [Fig. 10(b)]. The large porosity implies a strong interaction between perforations, which Betts included in his model using the inverse of Fok's function.[19] The importance of including hole interaction effects in the modeling of perforated plates with bias flow is emphasized by the greater accuracy in which Betts' model[27] and the proposed model [Eq. (33)] predict the insertion loss measurements versus the models of Howe and Jing and Sun.

Figure 10(a) indicates that all preceding models[9,10,27] do not resolve the saturation and decline in L_I that is characteristic of standing-wave resonance in the perforations. The error between both Howe[9] and Jing and Sun's[10] theory with the current experiments can be attributed to the low porosity approximations made in their works. Although Bett's model includes interaction effects, the discrepancy within previously validated d/λ [Fig. 8(a)] is substantial. By substituting the constant valued discharge coefficient in Bett's model [Eq. (9)] with Eq. (17), the agreement between measurements from this study and Bett's model can be significantly improved (Fig. 11). This emphasizes the importance in considering discharge coefficient variations with bias flow and perforation geometry, and underpins an advantage of the proposed model [Eq. (33)] over previous models.[9,10,27]

It is emphasized that the aforementioned models[9,10,27] were developed with the goal of optimizing aircraft engine liners. The liner assembly employs perforations with around 5% open area, hole diameter and plate thickness on the order of 1 mm, and is tuned to suppress targeted frequencies, such as the blade passage frequencies of a rotor.[39] At low porosity, interaction effects would have negligible influence on

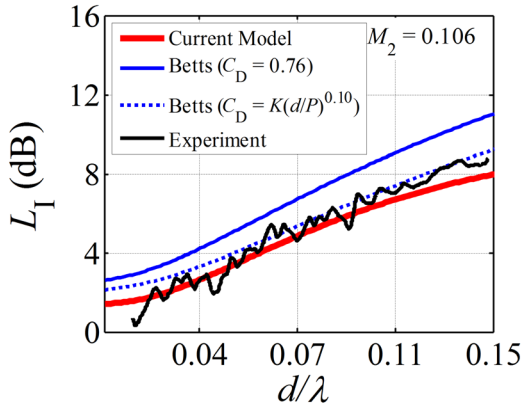

FIG. 11. (Color online) Insertion loss prediction using Betts' impedance model (see Ref. 27), comparing the use Eq. (17) and 0.76 for the discharge coefficient.

the transmission properties through the perforations.[10] The targeted frequencies for muffler silencing[39] are typically on the order of 5 kHz, and the corresponding plate thickness to wavelength ratio is large enough such that standing-wave-formed resonance in the perforations is unimportant. Therefore, models developed for the design of acoustic liners are not expected to resolve hole-interaction or standing-wave-formed resonance effects.

C. Accuracy of proposed model

To assess the range of validity of the current predictive model, the deviation between Eq. (33) and experiment was examined systematically. The insertion loss error is defined as

$$\Delta L_I = L_{I,\text{model}} - L_{I,\text{exp}}. \tag{40}$$

The transmitted acoustic signal from our experiments were first scaled up by a factor of four to reflect the full-scale frequencies corresponding to the bleed valve application motivating this study.[15] The full-scale, narrowband power level spectra were then discretized into $\frac{1}{3}$-octave bands (see for example, Ref. 40). Equation (40) was used to evaluate the performance of Eq. (33) for all plates tested in this study. Figure 12 summarizes the results, where the maximum error, $|\Delta L_{\text{I,max}}|$, is plotted with respect to M_2 for all perforated samples. $|\Delta L_{\text{I,max}}|$ was determined for $d/\lambda < 0.5$ to exclude large

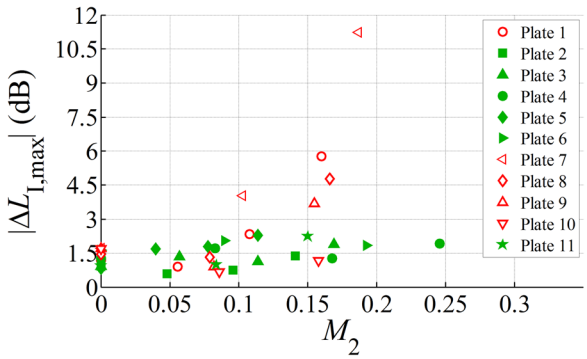

FIG. 12. (Color online) Maximum of insertion loss error Eq. (40) versus perforation Mach number. The open symbols are perforations with dimensionless thickness values within the range $0.5 < l/d < 0.8$.

error magnitudes from non-planar modes. The accuracy of the proposed model in predicting static insertion loss is demonstrated in Fig. 12, where deviations between Eq. (33) and experiment are less than 1.6 dB at $M_2 = 0$. The open symbols representing plates 1, 7, 8, and 9 indicate a substantially larger increase in $|\Delta L_{\text{I,max}}|$ with increasing M_2 than for the remaining plates. The large error can be explained by the assumption of a stable *vena contracta* downstream of the perforated plate. The location of the *vena contracta* was determined using the jet profile by Rouse and Abul-Fetouh,[33] and was assumed steady. Also, Rouse and Abul-Fetouh's analysis was based on a free jet issuing from a sharp edged orifice. The orifice thickness, which was not considered in their analysis,[33] can have significant impact on the details of the jet profile. Smith[41] described multiple flow regimes for a single orifice in a duct that depend on l/d. For thickness-to-orifice diameter ratio $0.5 < l/d < 0.8$, the jet may intermittently detach and reattach to the wall of the orifice. Plates 1, 7, 8, and 9 fall within this transitional regime, where the *vena contracta* location becomes unsteady. Since both the insertion loss and end correction in this study are modeled with the assumption of steady flow, the large discrepancies between model predictions and measurements for plates 1, 7, 8, and 9 can be attributed to separation/reattachment described by Smith. Plate 10 falls at the boundary of the transitional regime ($l/d < 0.8$); however, the growth in $|\Delta L_{\text{I,max}}|$ is not observed as with plates 1, 7, 8, and 9. The aforementioned range $0.5 < l/d < 0.8$ was determined for a single orifice in a duct. It is likely that mutual entrainment by neighboring perforations relocates the *vena contracta* position further upstream such that the jet successfully attaches to the downstream perforation rim. The *vena contracta* location is therefore stable and consistent with the steady flow assumption in this study.

The experimental results of this study are based on measurements of sound propagation within a duct. Although the acoustic liner in the duct minimizes internal reflections, non-planar acoustic modes are sustainable in the regions upstream and downstream of the perforated plate. Despite the propagation of non-planar modes, the experimental measurements in this study are in quantitative agreement with static one-dimensional measurements reported in Ref. 1 for the same perforated plates. The applicability of one-dimensional theory is assessed by examining d/λ_{max} for each plate. From Table III, the maximum resolved d/λ for plates 1, 3, 4, 8, 9, 10, and 11 is well below the cut-on criterion for non-planar modes [Eq. (39)]. Plates 2, 5, 6, and 7 can support non-planar modes, but only where $d/\lambda > 0.586(1-M^2)^{1/2}$. This means that, despite the non-uniform incident field upstream of the perforations, non-planar modes are cut off over a considerable range of resolved frequencies for plates 2, 5, 6, and 7, and are cut off at all resolved frequencies for the remaining plates. Given the frequency range and plate selections of the current study, the planar acoustic mode dominates the transmission process and the use of one-dimensional acoustic theory holds satisfactorily in this work.

The current analysis is valid only in quantifying the amount of transmitted energy from a known source upstream

of the perforation. Noise generation as a result of turbulence fluctuations can be a significant component of the total noise downstream of the perforation. A complete model for the sound emerging from perforated plates with bias flow would need to include both the propagation component and the generation of turbulent mixing noise. The latter could be an empirical model based on the vast literature on measurements and models of turbulent mixing noise from jets.[42–47] It would be reasonable to start this modeling process by assuming that the propagated noise and the generated noise are uncorrelated, in which case the intensity of the total field is simply the sum of the intensities of the two components. However, it is possible that the incident sound may induce forcing of the jets emerging from the perforations. In that case the turbulent mixing noise and propagated field could be coupled, resulting in a much more complex problem.

V. CONCLUSIONS

An experimental and theoretical parametric study of the acoustic damping characteristics of perforated plates at normal incidence with bias flow was conducted. The bias flow model developed in this study is based on one-dimensional wave propagation and mean flow through a single contraction/expansion chamber. The proposed model addresses certain aspects which previous models fail to investigate, by detailing effects of bias flow on the *vena contracta* and end corrections of a perforated plate. The *vena contracta* of the jet that forms due to flow separation from the upstream corner of the contraction was modeled as an additional area reduction to the physical area contraction. The mean flow upstream of the contraction is approximately potential, and therefore the mass end correction upstream of the contraction was assumed equal to the end correction length used in classical studies without flow. The mean flow downstream of the *vena contracta* is no longer potential due to the mixing process between the jet and surrounding fluid. The end correction downstream of the contraction was therefore modified assuming that the attached mass downstream of the *vena contracta* location is destroyed. The bias flow mixing and viscous dissipation are sources of irreversible losses, which were included in the insertion loss model through entropy fluctuations.

The proposed model [Eq. (33)] indicates a saturation and decline in insertion loss corresponding to standing-wave-formed resonance in the perforations as the acoustic wavelength approaches the thickness of the perforated plate. The dependence of resonant conditions on the plate thickness emphasizes the importance of accurately modeling the end correction of the perforated plate. A monotonic increase in the insertion loss at low frequencies is observed for increasing flow Mach number through the perforations. The acoustic losses are a result of the vortical mixing region downstream of the area expansion.

The experimental measurements obtained in this investigation confirm the trends observed in the proposed model for perforation Mach number $M_2 < 0.25$. At larger M_2, pressure fluctuations from the mean flow may become significant such that a further increase in the bias flow Mach number results in a decrease in the sound attenuation capability of the perforated plate. For perforates outside the range of dimensionless thickness $0.5 < l/d < 0.8$, the proposed model agrees with experimental data to within 2 dB within the range of dimensionless frequencies $d/l \leq 0.5$. Within the same range of d/l validated by previous models, the proposed model yields superior insertion loss predictions over previous models. The proposed model in this work extends predictions over a range of porosity and acoustic frequencies not covered by previous models.

NOMENCLATURE

A	area
a	perforation radius
c	wave propagation speed
C_c	contraction coefficient
C_D	discharge coefficient
d	perforation diameter
D	diameter upstream of perforated plate or contraction
f	frequency
i	$\sqrt{-1}$
I	incident pressure amplitude
IL	sound intensity level
J	acoustic energy flux
k	acoustic wave number
K_R	Rayleigh conductivity
l	plate thickness
l'	end correction length
L_I	insertion loss
L_T	transmission loss
$\dot{m}$	mass flow rate
M	Mach number
p	static pressure
p'	acoustic pressure
P	hole spacing between perforations
R	reflected wave amplitude
Re	Reynolds number
St	Strouhal number
t	time
T	transmitted pressure amplitude
T_c	transmission coefficient
u'	particle velocity
x	axial coordinate
z	normalized perforation impedance $= Z/\rho c$
Z	perforation impedance
β	perforation porosity
γ	specific heat ratio c_p/c_v
ΔL_I	insertion loss level difference between model and experiment
ε	perforation thickness correction
η	Stokes number
λ	acoustic wavelength
μ	dynamic viscosity of air
ν	kinematic viscosity of air
ξ	ratio of hole diameter to hole separation distance
Π	acoustic power
ρ	density
ψ	inverse of Fok's function

θ incidence angle between microphone tip and center of perforated plate
ω angular frequency

Subscripts

0 baseline (absent of perforation or contraction)
1 region upstream of contraction
2 region inside contraction
3 region downstream of contraction
c cutoff
e effective
exp experimental
i incident
j circumferential mode number
k radial mode number
m mixing
p perforation
ref reference value
t transmitted
vc *vena contracta*

[1]V. Phong and D. Papamoschou, "High frequency acoustic transmission loss of perforated plates at normal incidence," J. Acoust. Soc. Am. **134**(2), 1090–1101 (2013).
[2]P. Mungur and G. M. L. Gladwell, "Acoustic wave propagation in a sheared fluid contained in a duct," J. Sound Vib. **9**(1), 28–48 (1969).
[3]D. Ronneberger, "Experimentelle Untersuchungen zum akustischen Reflexionfaktor von unstetigen Querschnittanderungen in einem luftdurchstromten Rohr" ("Experimental investigations about the acoustic reflection coefficient of discontinuous changes of cross-section in tubes with air flow"), Acustica **19**, 222–235 (1967)
[4]R. J. Alfredson and P. O. A. L. Davies, "Performance of exhaust silencer components," J. Sound Vib. **15**(2), 175–196 (1971).
[5]P. O. A. L. Davies, "Practical flow duct acoustics," J. Sound Vib. **124**(1), 91–115 (1988).
[6]A. Cummings, "Sound transmission at sudden area expansions in circular ducts, with superimposed mean flow," J. Sound Vib. **38**(1), 149–155 (1975).
[7]G. C. G. Hofmans, R. J. J. Boot, P. P. J. M. Durrieu, Y. Aurégan, and A. Hirschberg, "Aeroacoustic response of a slit-shaped diaphragm in a pipe at low Helmholtz number, 1: Quasi-steady results," J. Sound Vib. **244**(1), 35–56 (2001).
[8]P. Durrieu, G. Hofmans, G. Ajello, R. Boot, Y. Aurégan, A. Hirschberg, and M. C. A. M. Peters, "Quasisteady aero-acoustic response of orifices," J. Acoust. Soc. Am. **110**(4), 1859–1872 (2001).
[9]M. S. Howe, "On the theory of unsteady high Reynolds number flow through a circular aperture," Proc. R. Soc. London **366**, 205–223 (1979).
[10]X. Jing and X. Sun, "Experimental investigation of perforated liners with bias flow," J. Acoust. Soc. Am. **106**(5), 2436–2441 (1999).
[11]X. Jing and X. Sun, "Effect of plate thickness on impedance of perforated plates with bias flow," AIAA J. **38**(1), 1573–1578 (2000).
[12]S. H. Lee, J. G. Ih, and K. S. Peat, "A model of acoustic impedance of perforated plates with bias flow considering the interaction effect," J. Sound Vib. **303**, 741–752 (2007).
[13]A. Mazdeh and R. Kashani, "Distributed parameter acoustic modeling of a perforation with bias flow," in *Proceedings of ASME Turbo Expo*, June 2011.
[14]S. Mendez and J. D. Eldredge, "Acoustic modeling of perforated plates with bias flow for Large-Eddy Simulations," J. Comput. Phys. **228**(13), 4757–4772 (2009).
[15]V. Phong, S. Taghavi Nezhad, and D. Papamoschou, "Noise reduction of a turbofan bleed valve," *50th AIAA Aerospace Sciences Meeting*, Nashville, TN, 2012.
[16]I. B. Crandall, *Theory of Vibration System and Sound* (Van Nostrand, New York, 1926), pp. 229.
[17]M. L. Munjal, *Acoustics of Ducts and Mufflers With Application to Exhaust and Ventilation System Design* (John Wiley and Sons, New York, 1987), Chap. 1, pp. 9–12.
[18]Lord Rayleigh, *The Theory of Sound* (Macmillan, Dover Publications, New York, 1945), Vol. II, Chap. 14, pp. 162–169.
[19]V. A. Fok, "Teoreticheskoe issledovanie provodimosti kruglogo otverstiya v perogorodke, postavlennoi poperek truby (Theoretical study of the conductance of a circular hole, in a partition across a tube, in Russian)," Dokl. Acad. Nauk SSSR **31**(9), 875–878 (1941).
[20]V. S. Nesterov, "(An experimental study of the acoustical conductivity of a circular orifice in a partition placed across a tube, in Russian)," Dokl. Acad. Nauk SSSR **31**(9), 879–882 (1941).
[21]J. Christensen, L. Martin-Moreno, and F. J. Garcia-Vidal, "Theory of resonant acoustic transmission through subwavelength apertures," Phys. Rev. Lett. **101**(1), 014301 (2008).
[22]B. Hou, J. Mei, M. Ke, W. Wen, Z. Liu, J. Shi, and P. Sheng, "Tuning Fabry-Perot resonances via diffraction evanescent waves," Phys. Rev. B **76**(5), 054303 (2007).
[23]B. Hou, J. Mei, M. Ke, Z. Liu, J. Shi, and W. Wen, "Experimental determination for resonance-induced transmission of acoustic waves through subwavelength hole arrays," J. Appl. Phys. **104**(1), 014909 (2008).
[24]A. Cummings and W. Eversman, "High amplitude acoustic transmission through duct terminations: Theory," J. Sound Vib. **91**(4), 503–518 (1983).
[25]I. J. Hughes and A. P. Dowling, "The absorption of sound by perforated linings," J. Fluid Mech. **218**, 299–335 (1990).
[26]J. D. Eldredge and A. P. Dowling, "The absorption of axial acoustic waves by a perforated liner with bias flow," J. Fluid Mech. **485**, 307–335 (2003).
[27]J. F. Betts, "Experiments and impedance modeling of liners including the effect of bias flow," Ph.D. thesis, Virginia Polytechnic Institute, Blacksburg, VA, 2000.
[28]J. H. Lienhard and J. H. Lienhard, "Velocity coefficients for free jets from sharp-edged orifices," J. Fluid. Eng. **106**, 13–17 (1984).
[29]P. L. Smith and M. Van Winkle, "Discharge coefficients through perforated plates at Reynolds numbers of 400 to 3,000," Am. Inst. Chem. Eng. J. **4**(3), 266–268 (1958).
[30]I. E. Idelchik, *Handbook of Hydraulic Resistance*, 2nd ed. (Hemisphere Publishing, Washington, DC, 1986), Chap. 4, pp. 135–188.
[31]R. Starobinski and Y. Aurégan, "Fluctuations of vorticity and entropy as sources of acoustical exergy," J. Sound Vib. **216**(3), 521–527 (1998).
[32]T. H. Melling, "The acoustic impedance of perforates at medium and high sound pressure levels," J. Sound Vib. **29**(1), 1–65 (1973).
[33]H. Rouse and A.-H. Abul-Fetouh, "Characteristics of irrotational flow through axially symmetric orifices," J. Appl. Mech. **17**(50), 421–426 (1950).
[34]C. H. Gerhold, L. R. Clark, M. H. Dunn, and J. Tweed, "Investigation of acoustical shielding by a wedge-shaped airframe," J. Sound Vib. **294**(1), 49–63 (2006).
[35]ISO 5136, *Acoustics - Determination of sound power radiated into a duct by fans and other air-moving devices - In-duct method* (International Organization for Standardization, Geneva, Switzerland, 2003).
[36]W. Neise and F. Arnold, "On sound power determination in flow ducts," J. Sound. Vib. **244**(3), 481–503 (2001).
[37]T. J. Mueller, C. S. Allen, W. K. Blake, R. P. Dougherty, D. Lynch, P. T. Soderman, and J. R. Underbrink, *Aeroacoustic Measurements* (Springer, Berlin, 2002), Ch. 1, pp. 3–13.
[38]T. Dassen, H. Holthusen, and M. Beukema, "Design and testing of a low self-noise aerodynamic microphone forebody," *2nd AIAA/CEAS Conference*, State College, PA, May 1996.
[39]M. J. T. Smith, *Aircraft Noise* (Cambridge University Press, Cambridge, UK, 2004), Ch. 4, pp. 144–150.
[40]D. Papamoschou and M. Debiasi, "Directional suppression of noise from a high-speed jet," AIAA J. **39**(3), 380–387 (2001).
[41]A. J. W. Smith, *Pressure Losses in Ducted Flows* (Butterworth and Co., London, UK, 1971), Chap. 4, pp. 135–188.
[42]M. E. Goldstein, "A generalized acoustic analogy," J. Fluid. Mech. **488**, 315–333 (2003).
[43]P. J. Morris and F. Farassat, "Acoustic analogy and alternative theories for jet noise prediction," AIAA J. **40**(4), 671–680 (2002).
[44]C. K. W. Tam and L. Auriault, "Jet mixing noise from fine-scale turbulence," AIAA J. **37**(2), 145–153 (1999).
[45]P. J. Morris, "A note on noise generation by large scale turbulent structures in subsonic and supersonic jets," Int. J. Aeroacoust. **8**(4), 301–316 (2009).
[46]R. Reba, S. Narayanan, and T. Colonius, "Wave-packet models for large-scale mixing noise," Int. J. Aeroacoust. **9**, 533–558 (2010), available at http://multi-science.atypon.com/doi/pdf/10.1260/1475-472X.9.4-5.533.
[47]T. Colonius, A. Samanta, and K. Gudmundsson, "Parabolized stability equation models of large-scale jet mixing noise," Proc. Eng. **6**, 64–73 (2010).